8

B-spline Shell Finite Element Updating by Means of Vibration Measurements

Antonio Carminelli and Giuseppe Catania
DIEM, Dept. of Mechanical Design, University of Bologna,
viale Risorgimento 2, 40136 Bologna,
Italy

1. Introduction

Within the context of structural dynamics, Finite Element (FE) models are commonly used to predict the system response. Theoretically derived mathematical models may often be inaccurate, in particular when dealing with complex structures. Several papers on FE models based on B-spline shape functions have been published in recent years (Kagan & Fischer, 2000; Hughes et al, 2005). Some papers showed the superior accuracy of B-spline FE models compared with classic polynomial FE models, especially when dealing with vibration problems (Hughes et al, 2009). This result may be useful in applications such as FE updating.

Estimated data from measurements on a real system, such as frequency response functions (FRFs) or modal parameters, can be used to update the FE model. Although there are many papers in the literature dealing with FE updating, several open problems still exist. Updating techniques employing modal data require a previous identification process that can introduce errors, exceeding the level of accuracy required to update FE models (D'ambrogio & Fregolent, 2000). The number of modal parameters employed can usually be smaller than that of the parameters involved in the updating process, resulting in ill-defined formulations that require the use of regularization methods (Friswell et al., 2001; Zapico et al.,2003). Moreover, correlations of analytical and experimental modes are commonly needed for mode shapes pairing. Compared with updating methods using modal parameters as input, methods using FRFs as input present several advantages (Esfandiari et al., 2009; Lin & Zhu, 2006), since several frequency data are available to set an over-determined system of equations, and no correlation analysis for mode pairing is necessary in general.

Nevertheless there are some issues concerning the use of FRF residues, such as the number of measurement degrees of freedom (dofs), the selection of frequency data and the ill-conditioning of the resulting system of equations. In addition, common to many FRF updating techniques is the incompatibility between the measurement dofs and the FE model dofs. Such incompatibility is usually considered from a dof number point of view only, measured dofs being a subset of the FE dofs. Reduction or expansion techniques are a common way to treat this kind of incompatibility (Friswell & Mottershead, 1995). A more general approach should also take into account the adoption of different dofs in the two models. As a matter of result, the adoption of B-spline functions as shape functions in a FE

model leads to non-physical dofs, and the treatment of this kind of coordinate incompatibility must be addressed.
In this paper a B-spline based FE model updating procedure is proposed. The approach is based on the least squares minimization of an objective function dealing with residues, defined as the difference between the model based response and the experimental measured response, at the same frequency. A proper variable transformation is proposed to constrain the updated parameters to lie in a compact domain without using additional variables. A B-spline FE model is adopted to limit the number of dofs. The incompatibility between the measured dofs and the B-spline FE model dofs is also dealt with.
An example dealing with a railway bridge deck is reported, considering the effect of both the number of measurement dofs and the presence on random noise. Results are critically discussed.

2. B-spline shell finite element model

2.1 B-spline shell model

A shell geometry can be efficiently described by means of B-spline functions mapping the parametric domain (ξ,η,τ) $(with\ 0 \le \xi,\eta,\tau \le 1)$ into the tridimensional Euclidean space (x,y,z). The position vector of a single B-spline surface patch, with respect to a Cartesian fixed, global reference frame ***O***, {x,y,z}, is usually defined by a tensor product of B-spline functions (Piegl & Tiller, 1997):

$$\mathbf{r}(\xi,\eta) = \begin{Bmatrix} r_x \\ r_y \\ r_z \end{Bmatrix} = \sum_{i=1}^{m}\sum_{j=1}^{n} B_i^p(\xi) \cdot B_j^q(\eta) \cdot \mathbf{P_{ij}}\,, \tag{1}$$

involving the following parameters:

- a control net of $m \times n$ Control Points (CPs) $\mathbf{P_{ij}}$;
- the uni-variate normalized B-spline functions $B_i^p(\xi)$ of degree *p*, defined with respect to the curvilinear coordinate ξ by means of the knot vector:

$$\mathbf{U} = \left\{\xi_1,\ldots,\xi_{m+p+1}\right\} = \left\{\underbrace{0,\ldots,0}_{p+1},\xi_{p+1},\ldots,\xi_m,\underbrace{1,\ldots,1}_{p+1}\right\};$$

- the uni-variate normalized B-spline functions $B_j^q(\eta)$ of degree *q*, defined with respect to the curvilinear coordinate η by means of the knot vector:

$$\mathbf{V} = \left\{\eta_1,\ldots,\eta_{n+q+1}\right\} = \left\{\underbrace{0,\ldots,0}_{q+1},\eta_{q+1},\ldots,\eta_n,\underbrace{1,\ldots,1}_{q+1}\right\}.$$

The degenerate shell model is a standard in FE software because of its simple formulation (Cook et al., 1989). The position vector of the solid shell can be expressed as:

$$\mathbf{s}(\xi,\eta,\tau) = \sum_{i=1}^{m}\sum_{j=1}^{n} B_i^p(\xi) \cdot B_j^q(\eta) \cdot \left[\mathbf{P_{ij}} + t_{ij}\left(\tau - \frac{1}{2}\right)\mathbf{v^3_{ij}}\right], \tag{2}$$

where the versors $\mathbf{v_{ij}^3}$ and the thickness values t_{ij} can be calculated from the interpolation process proposed in (Carminelli & Catania, 2009).
The displacement field can be defined by following the isoparametric approach and enforcing the fiber inextensibility in the thickness direction (Cook et al., 1989):

$$\mathbf{d}(\xi,\eta,\tau)=\begin{Bmatrix} d_x \\ d_y \\ d_z \end{Bmatrix}=\sum_{i=1}^{m}\sum_{j=1}^{n} B_i^p(\xi)\cdot B_j^q(\eta)\cdot\left(\begin{Bmatrix} \mathrm{u_{ij}} \\ \mathrm{v_{ij}} \\ \mathrm{w_{ij}} \end{Bmatrix}+\mathrm{t}_{ij}\left(\tau-\frac{1}{2}\right)[\mathbf{-v_{ij}^2}\quad \mathbf{v_{ij}^1}]\begin{Bmatrix}\alpha_{\mathbf{ij}}\\ \beta_{\mathbf{ij}}\end{Bmatrix}\right)=$$

$$=\sum_{i=1}^{m}\sum_{j=1}^{n} B_i^p(\xi)\cdot B_j^q(\eta)\cdot\begin{bmatrix} 1 & 0 & 0 & & \\ 0 & 1 & 0 & \mathrm{t}_{ij}\left(\tau-\frac{1}{2}\right)[\mathbf{-v_{ij}^2}\quad \mathbf{v_{ij}^1}] \\ 0 & 0 & 1 & & \end{bmatrix}\cdot\begin{Bmatrix} \mathrm{u_{ij}} \\ \mathrm{v_{ij}} \\ \mathrm{w_{ij}} \\ \alpha_{\mathbf{ij}} \\ \beta_{\mathbf{ij}} \end{Bmatrix}= \tag{3}$$

$$=\begin{bmatrix} \mathbf{N_u} \\ \mathbf{N_v} \\ \mathbf{N_w} \end{bmatrix}\cdot\boldsymbol{\delta}=\mathbf{N}\cdot\boldsymbol{\delta}\,,$$

where $\boldsymbol{\delta}$ is the vector collecting the $(5\cdot m\cdot m)$ generalized dofs:

$$\boldsymbol{\delta}^T=\{u_{11}\quad v_{11}\quad w_{11}\quad \alpha_{11}\quad \beta_{11}\quad\cdots\quad u_{mn}\quad v_{mn}\quad w_{mn}\quad \alpha_{mn}\quad \beta_{mn}\}\,, \tag{4}$$

$\left(\mathbf{v_{ij}^1},\mathbf{v_{ij}^2},\mathbf{v_{ij}^3}\right)$ refer to orthonormal sets defined on $\mathbf{P}_{ij}$ starting from the vector $\mathbf{v_{ij}^3}$ (Carminelli & Catania, 2007), $\mathrm{u_{ij}}$, $\mathrm{v_{ij}}$ and $\mathrm{w_{ij}}$ are translational dofs, $\alpha_{\mathbf{ij}}$ and $\beta_{\mathbf{ij}}$ are rotational dofs.
The strains can be obtained from displacements in accordance with the standard positions assumed in three-dimensional linear elasticity theory (small displacements and small deformations), and can be expressed as:

$$\boldsymbol{\varepsilon}=\begin{Bmatrix}\varepsilon_x & \varepsilon_y & \varepsilon_z & \gamma_{xy} & \gamma_{yz} & \gamma_{xz}\end{Bmatrix}^T=\mathbf{L}\cdot\mathbf{N}\cdot\boldsymbol{\delta}=\mathbf{D}\cdot\boldsymbol{\delta}\,, \tag{5}$$

where $\mathbf{D=L\cdot N}$ and $\mathbf{L}$ is the linear operator:

$$\mathbf{L}=\begin{bmatrix} \frac{\partial}{\partial x} & 0 & 0 & \frac{\partial}{\partial y} & 0 & \frac{\partial}{\partial z} \\ 0 & \frac{\partial}{\partial y} & 0 & \frac{\partial}{\partial x} & \frac{\partial}{\partial z} & 0 \\ 0 & 0 & \frac{\partial}{\partial z} & 0 & \frac{\partial}{\partial y} & \frac{\partial}{\partial x} \end{bmatrix}^T. \tag{6}$$

The stress tensor $\boldsymbol{\sigma}$ and strain $\boldsymbol{\varepsilon}$ are related by the material constitutive relationship:

$$\boldsymbol{\sigma}=\begin{Bmatrix}\sigma_x & \sigma_y & \sigma_z & \tau_{xy} & \tau_{yz} & \tau_{xz}\end{Bmatrix}^T=\mathbf{E}\cdot\boldsymbol{\varepsilon}\,, \tag{7}$$

where **E** is the plane stress constitutive matrix obtained according to the Mindlin theory. **T** is the transformation matrix from the local material reference frame (1,2,3) to the global reference frame (x,y,z) (Cook et al., 1989):

$$\mathbf{E} = \mathbf{T}^{\mathbf{T}} \cdot \mathbf{E}' \cdot \mathbf{T}\,, \tag{8}$$

and $\mathbf{E}'$ is the plane stress constitutive matrix in the local material reference frame:

$$\mathbf{E}' = \begin{bmatrix} \frac{E_1}{\left(1-\nu_{12}\nu_{21}\right)} & \frac{\nu_{12}E_2}{\left(1-\nu_{12}\nu_{21}\right)} & 0 & 0 & 0 & 0 \\ \frac{\nu_{12}E_2}{\left(1-\nu_{12}\nu_{21}\right)} & \frac{E_2}{\left(1-\nu_{12}\nu_{21}\right)} & 0 & 0 & 0 & 0 \\ 0 & 0 & 0 & 0 & 0 & 0 \\ 0 & 0 & 0 & G_{12} & 0 & 0 \\ 0 & 0 & 0 & 0 & G_{23} & 0 \\ 0 & 0 & 0 & 0 & 0 & G_{13} \end{bmatrix}, \tag{9}$$

where E_{ij} are Young modulus, G_{ij} are shear modulus and v_{ij} are Poisson's ratios in the material reference frame.

The expressions of the elasticity, inertia matrices and of the force vector can be obtained by means of the principle of minimum total potential energy:

$$\Pi = U + W \rightarrow \min\,, \tag{10}$$

where U is the potential of the strain energy of the system:

$$U = \frac{1}{2}\int_{\Omega} \boldsymbol{\varepsilon}^{\mathbf{T}} \cdot \boldsymbol{\sigma}\; d\Omega\,, \tag{11}$$

and W is the potential of the body force **f** and of the surface pressure Q, and includes the potential W_i of the inertial forces:

$$W = -\int_{\Omega} \mathbf{d}^{\mathbf{T}} \cdot \mathbf{f} \cdot d\Omega - \int_{S} \mathbf{d}^{\mathbf{T}} \cdot \mathbf{Q} \cdot dS + W_i\,, \tag{12}$$

where:

$$W_i = \int_{\Omega} \rho \cdot \mathbf{d}^{\mathbf{T}} \cdot \ddot{\mathbf{d}} \cdot d\Omega\,. \tag{13}$$

The introduction of the displacement function (Eq.3) in the functional Π (Eq.10), imposing the stationarity of the potential energy:

$$\nabla_{\boldsymbol{\delta}}\left(\Pi\right) = 0\,, \tag{14}$$

yields the equations of motion:

$$\mathbf{M} \cdot \ddot{\boldsymbol{\delta}} + \mathbf{K}_{\mathbf{f}} \cdot \boldsymbol{\delta} = \mathbf{F}\,, \tag{15}$$

where the unconstrained stiffness matrix is:

$$\mathbf{K_f} = \int_{\Omega} \mathbf{D^T} \cdot \mathbf{E} \cdot \mathbf{D}\, d\Omega\,, \tag{16}$$

the mass matrix is:

$$\mathbf{M} = \int_{\Omega} \rho \cdot \mathbf{N^T} \cdot \mathbf{N}\, d\Omega\,, \tag{17}$$

and the force vector is:

$$\mathbf{F} = \int_{\Omega} \mathbf{N^T} \cdot \mathbf{f}\; d\Omega + \int_{S} \mathbf{N^T} \cdot \mathbf{Q}\; dS\,, \tag{18}$$

where ρ is the mass density, Ω being the solid structure under analysis and S the external surface of solid Ω.

2.2 Constraint modeling

Distributed elastic constraints are taken into account by including an additional term ΔW in the functional of the total potential energy. The additional term ΔW takes into account the potential energy of the constraint force per unit surface area Q_C, assumed as being applied on the external surface of the shell model:

$$\mathbf{Q_C} = -\mathbf{R} \cdot \mathbf{d}\,, \tag{19}$$

where **R** is the matrix containing the stiffness coefficients r_{ab} of a distributed elastic constraint, modeled by means of B-spline functions:

$$r_{ab} = \sum_{i=1}^{m^{ab}} \sum_{j=1}^{n^{ab}} B_i^{p^{ab}} \cdot B_j^{q^{ab}} \cdot \kappa_{\mathrm{ij}}^{ab}\,, \tag{20}$$

where $B_i^{p^{ab}}$ and $B_j^{q^{ab}}$ are the uni-variate normalized B-spline functions defined by means of the knot vectors, respectively, $\mathbf{U^{ab}}$ and $\mathbf{V^{ab}}$:

$$\Delta W = -\frac{1}{2}\int_S (\mathbf{d}^T \cdot \mathbf{Q_C})\, dS = \frac{1}{2}\boldsymbol{\delta}^{\mathbf{T}} \cdot \int_S \left(\mathbf{N^T} \cdot \mathbf{R} \cdot \mathbf{N}\right) dS \cdot \boldsymbol{\delta}\,. \tag{21}$$

The stiffness matrix due to the constraint forces is

$$\boldsymbol{\Delta K} = \int_S \left(\mathbf{N^T} \cdot \mathbf{R} \cdot \mathbf{N}\right) dS\,. \tag{22}$$

The introduction of ΔW this last term in the total potential energy Π yields the equation of motion:

$$\mathbf{M} \cdot \ddot{\boldsymbol{\delta}} + \left(\mathbf{K_f} + \boldsymbol{\Delta K}\right) \cdot \boldsymbol{\delta} = \mathbf{F}\,. \tag{23}$$

2.3 Damping modelling

For lightly damped structures, effective results may be obtained by imposing the real damping assumption (real modeshapes).

The real damping assumption is imposed by adding a viscous term in the equation of motion:

$$\mathbf{M}\cdot\ddot{\boldsymbol{\delta}}+\mathbf{C}\cdot\dot{\boldsymbol{\delta}}+\left(\mathbf{K_f}+\mathbf{\Delta K}\right)\cdot\boldsymbol{\delta}=\mathbf{F}\,, \tag{24}$$

where the damping matrix **C** is:

$$\mathbf{C}=\boldsymbol{\Phi}^{-T}\cdot\mathbf{diag}(2\zeta\omega)\cdot\boldsymbol{\Phi}^{-1}\,, \tag{25}$$

and

$$\mathbf{diag}(2\zeta\omega)=\begin{bmatrix}2\zeta_1\omega_1 & 0 & \cdots & 0\\ 0 & 2\zeta_2\omega_2 & & \vdots\\ \vdots & & \ddots & 0\\ 0 & \cdots & 0 & 2\zeta_N\omega_N\end{bmatrix}, \tag{26}$$

where $\boldsymbol{\Phi}$ is the matrix of the eigen-modes $\boldsymbol{\Phi}_i$ obtained by solving the eigen-problem:

$$\left(\mathbf{K}-\omega_i^2\mathbf{M}\right)\boldsymbol{\Phi}_i=\mathbf{0}\,, \tag{27}$$

and ω_i^2 is the i-th eigen-value of Eq.(27). Modal damping ratios ζ_i can be evaluated from:

$$\zeta_i=\zeta\left(f_i\right)=\zeta\left(2\pi\cdot\omega_i\right), \tag{28}$$

where the damping $\zeta(f)$ is defined by means of control coefficients γ_z and B-spline functions B_z defined on a uniformly spaced knot vector:

$$\zeta\left(f\right)=\zeta\left(f(u)\right)=\sum_{z=1}^{n^z}B_z(u)\cdot\gamma_z;\quad f=f_{ST}+u\cdot\left(f_{FI}-f_{ST}\right);\quad u\in[0,1], \tag{29}$$

where f_{ST} and f_{FI} are, respectively, the lower and upper bound of the frequency interval in which the spline based damping model is defined.

3. Updating procedure

The parametrization adopted for the elastic constraints and for the damping model is employed in an updating procedure based on Frequency Response Functions (FRFs) experimental measurements.

The ℓ measured FRFs $H_b^X(\omega)$, with $b=1,\ldots,\ell$, are collected in a vector $\mathbf{h}_X(\omega)$:

$$\mathbf{h}_X(\omega)=\begin{Bmatrix}H_1^X(\omega)\\ \vdots\\ H_\ell^X(\omega)\end{Bmatrix}. \tag{30}$$

The dynamic equilibrium equation in the frequency domain, for the spline-based finite element model, can be defined by Fourier transforming Eq.(24), where $\mathsf{F}(\,)=\tilde{(\,)}$:

$$\left(-\omega^2\mathbf{M}+j\omega\mathbf{C}+\mathbf{K_f}+\Delta\mathbf{K}\right)\cdot\tilde{\boldsymbol{\delta}}=\mathbf{Z}(\omega)\cdot\tilde{\boldsymbol{\delta}}=\mathbf{H}^{-1}(\omega)\cdot\tilde{\boldsymbol{\delta}}=\tilde{\mathbf{F}}\,, \tag{31}$$

where $\mathbf{Z}(\omega)$ is the dynamic impedance matrix and $\mathbf{H}(\omega)=(\mathbf{Z}(\omega))^{-1}$ is the receptance matrix. Since the vector $\tilde{\boldsymbol{\delta}}$ contains non-physical displacements and rotations, the elements of the matrix $\mathbf{H}(\omega)$ cannot be directly compared with the measured FRFs $H_q^X(\omega)$. The analytical FRFs related to physical dofs of the model can be obtained by means of the FE shape functions. Starting from the input force applied and measured on the point $\mathbf{P^i}=\mathbf{s}(\xi_i,\eta_i,\tau_i)$ along a direction $\boldsymbol{\varphi}$ and the response measured on the point $\mathbf{P^r}=\mathbf{s}(\xi_r,\eta_r,\tau_r)$ along the direction $\boldsymbol{\psi}$, the corresponding analytical FRF is:

$$H_{\boldsymbol{\psi},\boldsymbol{\varphi}}^{r,i}(\omega)=\mathbf{N}_{\boldsymbol{\psi}}(\xi_r,\eta_r,\tau_r)\cdot\mathbf{H}(\omega)\cdot\mathbf{N}_{\boldsymbol{\varphi}}^T(\xi_i,\eta_i,\tau_i)\,, \tag{32}$$

where $\boldsymbol{\varphi}$ and $\boldsymbol{\psi}$ can assume a value among **u**, **v** or **w** (Eq.3).
The sensitivity of the FRF $H_{\boldsymbol{\psi},\boldsymbol{\varphi}}^{r,i}$ with respect to a generic parameter p_k is:

$$\begin{aligned}\frac{\partial H_{\boldsymbol{\varphi},\boldsymbol{\psi}}^{i,s}(\omega,\mathbf{p})}{\partial p_k}&=\mathbf{N}_{\boldsymbol{\psi}}(\xi_r,\eta_r,\gamma_r)\cdot\frac{\partial\mathbf{H}(\omega,\mathbf{p})}{\partial p_k}\cdot\mathbf{N}_{\boldsymbol{\varphi}}^T(\xi_i,\eta_i,\gamma_i)=\\&=-\mathbf{N}_{\boldsymbol{\psi}}(\xi_r,\eta_r,\gamma_r)\cdot\mathbf{H}(\omega,\mathbf{p})\cdot\frac{\partial\mathbf{Z}(\omega,\mathbf{p})}{\partial p_k}\cdot\mathbf{H}(\omega,\mathbf{p})\cdot\mathbf{N}_{\boldsymbol{\varphi}}^T(\xi_i,\eta_i,\gamma_i),\end{aligned} \tag{33}$$

where $\mathbf{p}=\left\{p_1\quad\cdots\quad p_{n^p}\right\}^T$ is the vector containing the updating parameters p_k.
Since each measured FRF $H_b^X(\omega)$ refers to a well-defined set $\{i,r,\boldsymbol{\varphi},\boldsymbol{\psi}\}$, it is possible to collect, with respect to each measured FRF, the analytical FRFs in the vector:

$$\mathbf{h_a}(\omega,\mathbf{p})=\begin{Bmatrix}H_{\boldsymbol{\varphi},\boldsymbol{\psi}}^{i,s}(\omega,\mathbf{p})\\\vdots\\H_{\boldsymbol{\theta},\boldsymbol{\sigma}}^{\ell,t}(\omega,\mathbf{p})\end{Bmatrix}. \tag{34}$$

The elements of $\mathbf{h}_a(\omega,\mathbf{p})$ are generally nonlinear functions of **p**. The problem can be linearized, for a given angular frequency ω_i, by expanding $\mathbf{h_a}(\omega,\mathbf{p})$ in a truncated Taylor series around $\mathbf{p}=\mathbf{p}_0$:

$$\mathbf{h_a}(\omega_i,\mathbf{p_o})+\sum_{k=1}^{n^p}\frac{\partial\mathbf{h_a}(\omega_i,\mathbf{p_o})}{\partial p_k}\Delta p_k=\mathbf{h_x}(\omega_i)\,, \tag{35}$$

in matrix form:

$$\left[\frac{\partial\mathbf{h_a}(\omega_i,\mathbf{p_o})}{\partial p_1},\cdots,\frac{\partial\mathbf{h_a}(\omega_i,\mathbf{p_o})}{\partial p_k},\ldots,\frac{\partial\mathbf{h_a}(\omega_i,\mathbf{p_o})}{\partial p_{np}}\right]\begin{bmatrix}\Delta p_1\\\vdots\\\Delta p_k\\\vdots\\\Delta p_{np}\end{bmatrix}=\mathbf{h_x}(\omega_i)-\mathbf{h_a}(\omega_i,\mathbf{p_o})\,, \tag{36}$$

or:

$$\mathbf{S}_i \cdot \mathbf{\Delta p} = \mathbf{\Delta h}_i \,, \tag{37}$$

where $\mathbf{S}_i$ is the sensitivity matrix for the *i-th* angular frequency value ω_i.
It is possible to obtain a least squares estimation of the n^p parameters p_k, by defining the error function **e**:

$$\mathbf{e} = \sum_{i=1}^{n^f} \mathbf{S}_i \cdot \mathbf{\Delta p} - \mathbf{\Delta h}_i \,, \qquad n^f \gg n^p \,, \tag{38}$$

and by minimizing the objective function *g*:

$$g = \left(\mathbf{e}^T \cdot \mathbf{e}\right) \rightarrow \min \,. \tag{39}$$

Since the updating parameters p_k belong to different ranges of value, ill-conditioned updating equations may result. A normalization of the variables was employed to prevent ill-conditioning of the sensitivity matrix:

$$p_k = p_{0_k} \cdot \left(1 + x_k\right) \quad ; \; k=1,\ldots,n^p \,, \tag{40}$$

where p_{0_k} is a proper normalization value for the parameter p_k.
Moreover, to avoid updating parameters assuming non-physical values during the iterative procedure, a proper variable transformation is proposed to constrain the parameters in a compact domain without using additional variables:

$$x_{k_{min}} \le x_k \le x_{k_{max}} \,, \quad \left(x_{k_{min}} = \frac{p_{k_{min}}}{p_{0_k}} - 1, \quad x_{k_{max}} = \frac{p_{k_{max}}}{p_{0_k}} - 1 \right) \,, \tag{41}$$

where $p_{k_{max}}$ and $p_{k_{min}}$ are, respectively, the maximum and minimum values allowed for the parameter p_k. The transformation is:

$$\begin{aligned} p_k &= p_{0_k} \cdot \left(1 + 0.5 \cdot \left(x_{k_{min}} + x_{k_{max}} + \left(x_{k_{max}} - x_{k_{min}}\right) \cdot \sin\left(y_k\right)\right)\right) = \\ &= p_{0_k} + 0.5 \cdot \left(p_{k_{min}} + p_{k_{max}} - 2 \cdot p_{0_k} + \left(p_{k_{max}} - p_{k_{min}}\right) \cdot \sin\left(y_k\right)\right) . \end{aligned} \tag{42}$$

The sensitivity matrices were derived with respect to the new variables y_k:

$$\frac{\partial \mathbf{h}_a}{\partial y_k} = \frac{\partial \mathbf{h}_a}{\partial p_k} \cdot \frac{\partial p_k}{\partial y_k} = 0.5 \cdot \left(p_{k_{max}} - p_{k_{min}}\right) \cdot \cos\left(y_k\right) \cdot \frac{\partial \mathbf{h}_a}{\partial p_k} \,, \tag{43}$$

which are allowed to take real values ($-\infty \le y_k \le \infty$) during the updating procedure.

Since FRF data available from measurement are usually large in quantity, a least squares estimation of the parameters can be obtained by adopting various FRF data at different frequencies. The proposed technique is iterative because a first order approximation was made during derivation of Eq.(35). At each step the updated global variables p_k can be obtained by means of Eq.(42).

4. Applications

The numerical example concerns the deck of the "Sinello" railway bridge (Fig.1). It is a reinforced concrete bridge located between Termoli and Vasto, Italy. It has been studied by several authors (Gabriele et al., 2009; Garibaldi et al., 2005) and design data and dynamical simulations are available.

The second deck span is a simply supported grillage with five longitudinal and five transverse beams. The grillage and the slab were modeled with an equivalent orthotropic plate, with fourth degree B-spline functions and 13x5 CPs (blue dot in Fig.2), for which the equivalent material properties were estimated by means of the design project:

$$E_1 = 5.5 \cdot 10^9\, Pa, \quad E_2 = 9.6 \cdot 10^8\, Pa, \quad G = 4.3 \cdot 10^8\, Pa,$$
$$\rho = 975\, Kg/m^3, \quad \nu_{12} = 0.3.$$

Because of FRF experimental measurement unavailability, two sets of experimental measurements were simulated assuming the input force applied on point 1 along z direction (Fig. 2). Twelve response dofs (along z direction) were used in the first set (red squares in Fig.2), while the second set contains only four measurement response dofs (red squares 1-4 in Fig. 2), in the frequency range [0, 80] Hz.

The simply supported constraint was modelled as a distributed stiffness acting on a portion of the bottom surface of the plate (τ = 0):

$$\mathbf{\Delta K} = \int_S (\mathbf{N}^T \cdot \mathbf{R} \cdot \mathbf{N}) \cdot dS\,, \tag{44}$$

where **R** is the matrix containing the stiffness of distributed spring acting only in vertical direction *z*:

$$\mathbf{R} = \begin{bmatrix} 0 & 0 & 0 \\ 0 & 0 & 0 \\ 0 & 0 & r_{33}(\xi,\eta) \end{bmatrix}. \tag{45}$$

The distributed stiffness r_{33} is modelled by means of B-spline functions:

$$r_{33} = \sum_{i=1}^{1}\sum_{j=1}^{4} B'^0_i(\xi) \cdot B'^2_j(\eta) \cdot \boldsymbol{\kappa}'_{ij} + \sum_{i=1}^{1}\sum_{j=1}^{4} B''^0_i(\xi) \cdot B''^2_j(\eta) \cdot \boldsymbol{\kappa}''_{ij}\,, \tag{46}$$

where:

- $\boldsymbol{\kappa}' = 10^9 \cdot [0.4 \quad 1.5 \quad 1.8 \quad 0.6] N/m^3$, and the associated B-spline functions are defined on the knot vectors $\mathbf{U}' = \{0, 0.03\}$ and $\mathbf{V}' = \{0,0,0,0.5,1,1,1\}$;
- $\boldsymbol{\kappa}'' = 10^9 \cdot [1.5 \quad 0.4 \quad 0.5 \quad 1.8] N/m^3$, and the associated B-spline functions are defined on the knot vectors $\mathbf{U}'' = \{0.97, 1\}$ and $\mathbf{V}'' = \{0,0,0,0.5,1,1,1\}$.

The distribution of the spring stiffness is plotted in Fig.3. In order to simplify the presentation of the numerical results, the stiffness coefficients are collected in the vector **κ** as follows:

$$\boldsymbol{\kappa} = [\boldsymbol{\kappa}' \quad \boldsymbol{\kappa}''] = [\kappa_1 \quad \cdots \quad \kappa_j \quad \cdots \quad \kappa_8] = 10^9 \cdot [0.4 \quad 1.5 \quad 1.8 \quad 0.6 \quad 1.5 \quad 0.4 \quad 0.5 \quad 1.8] N/m^3\,. \tag{47}$$

The modal damping ratio values reported in Fig.4 were employed for the first 30 eigen-modes.

Fig. 1. Sinello railway bridge (Garibaldi et al., 2005).

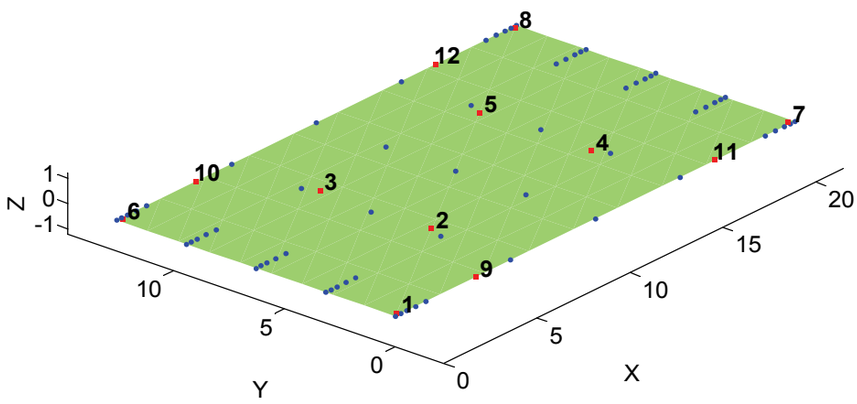

Fig. 2. The B-spline FE model with the 13x5 pdc (blue dot) and the 12 measurement response dofs (red squares).

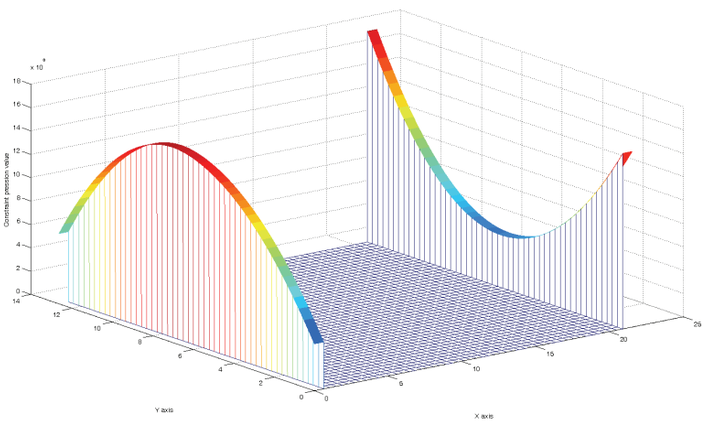

Fig. 3. Distributed stiffness values (vertical-axis) of the simply supported constraint employed to generate the measurements.

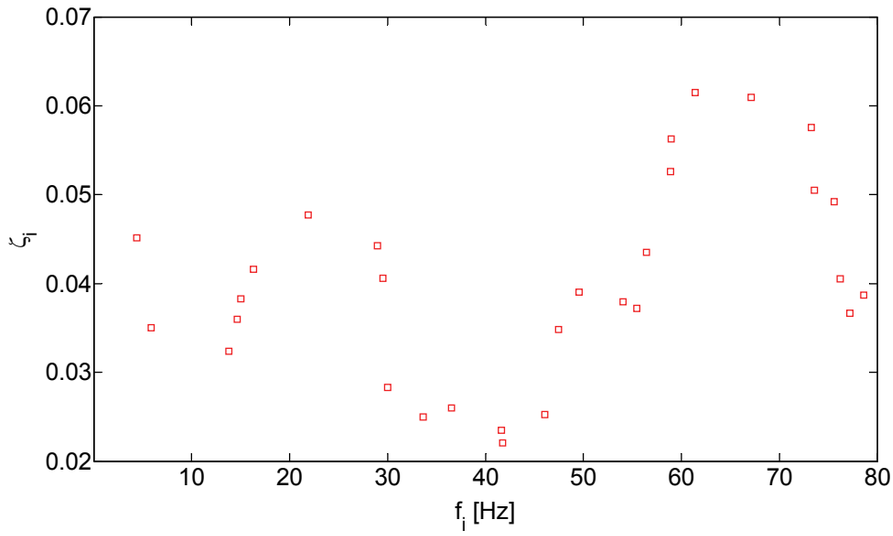

Fig. 4. Modal damping ratio values adopted to simulate the measurements. The values refer to the first 30 modes in the frequency range [0,80] Hz.

4.1 Numerical simulation without noise and with 12 measurement response dofs

Coefficients in vector $\boldsymbol{\kappa}$ and damping coefficients γ_z (quadratic B-spline functions, n^z=7, f_{ST}=0 Hz and f_{FI}=80 Hz in Eq.28) are assumed as the updating identification variables. The updating procedure is started by setting all of the coefficients in $\boldsymbol{\kappa}$ to 10^9 N/m^3 and all of the damping coefficients to 0.01. The comparison of the resulting FRFs is reported in Fig.5. The gradient of $\mathbf{C}$ with respect to the stiffness parameters is disregarded, i.e. $\frac{\partial \mathbf{C}}{\partial p_k} \simeq 0$ if $p_k \neq \gamma_z$. All twelve measurements dofs (Fig. 2) are considered as input. The value of the identification parameters at each step, adopting the proposed procedure, is reported in Fig.6 for the stiffness coefficients, and in Fig.7 for the γ_z coefficients; Fig.8 refers to the comparison of the modal damping ratio values used to simulate the measurements (red squares) and the identified curve (black line). The negative values of some parameters can lead to non physical stiffness matrix $\Delta\mathbf{K}$ so that instabilities may occur during the updating procedure. The proposed variable transformation does not allow stiffness coefficients to assume negative values. The comparison of theoretical and input FRF after updating is reported in Fig.9.

4.2 Numerical simulation without noise and with 4 measurement response dofs

The second simulation deals with the same updating parameters adopted in the previous example and with the same starting values, but only four measurement response dofs (dofs from 1 to 4 in Fig. 2) are considered.

The value of the identification parameters at each step, adopting the proposed procedure, is reported in Fig.10 for the stiffness coefficients, and in Fig.11 for the γ_z damping coefficients; Fig.12 refers to the comparison of the modal damping ratio values used to simulate the measurements (red squares) and the identified curve (black line). Fig.13 refers to the comparison of the FRFs after updating.

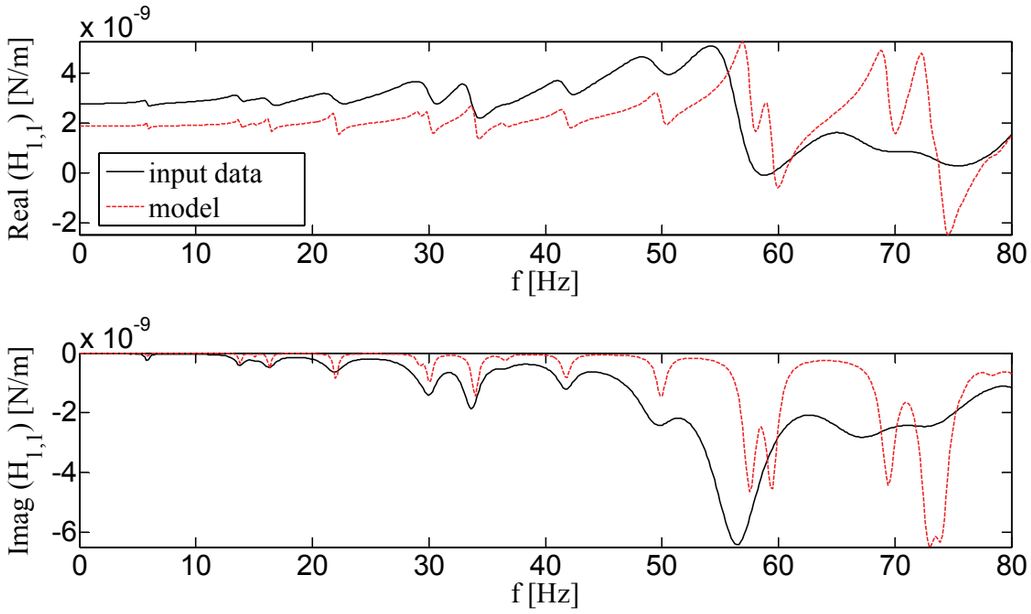

Fig. 5. Comparison of (input in dof 1; output in dof 1) FRF before updating: the input data (black continuous line) and the model (red dotted line).

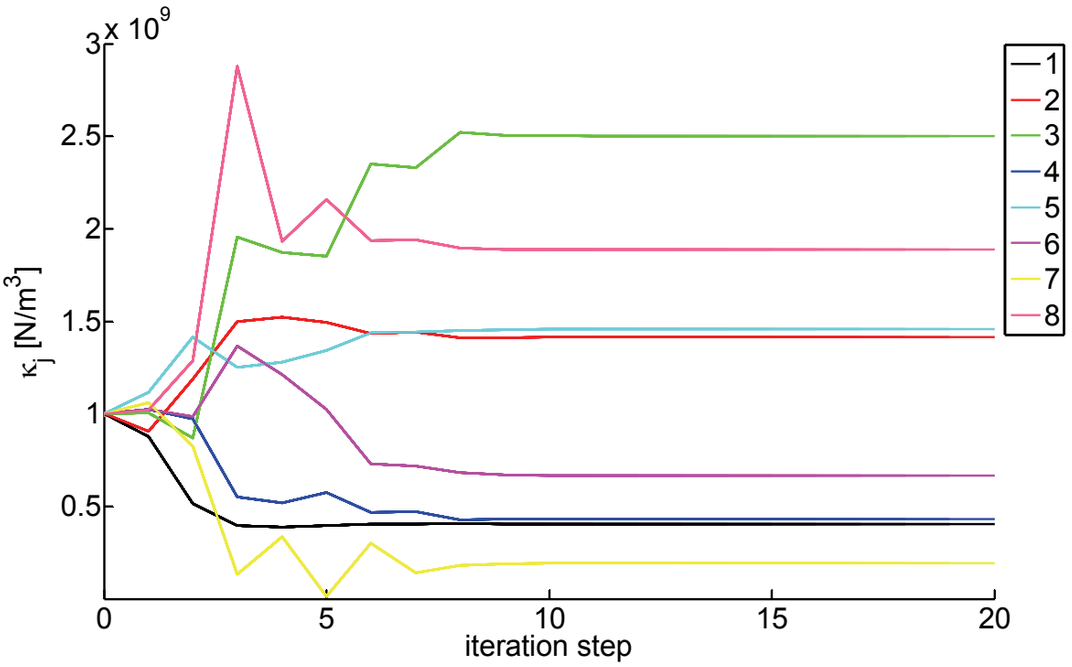

Fig. 6. Evolution of the stiffness parameters κ_j (j=1,...,8 in the legend) during iterations by adopting the proposed updating procedure. Example with 12 measurement response dofs and without noise.

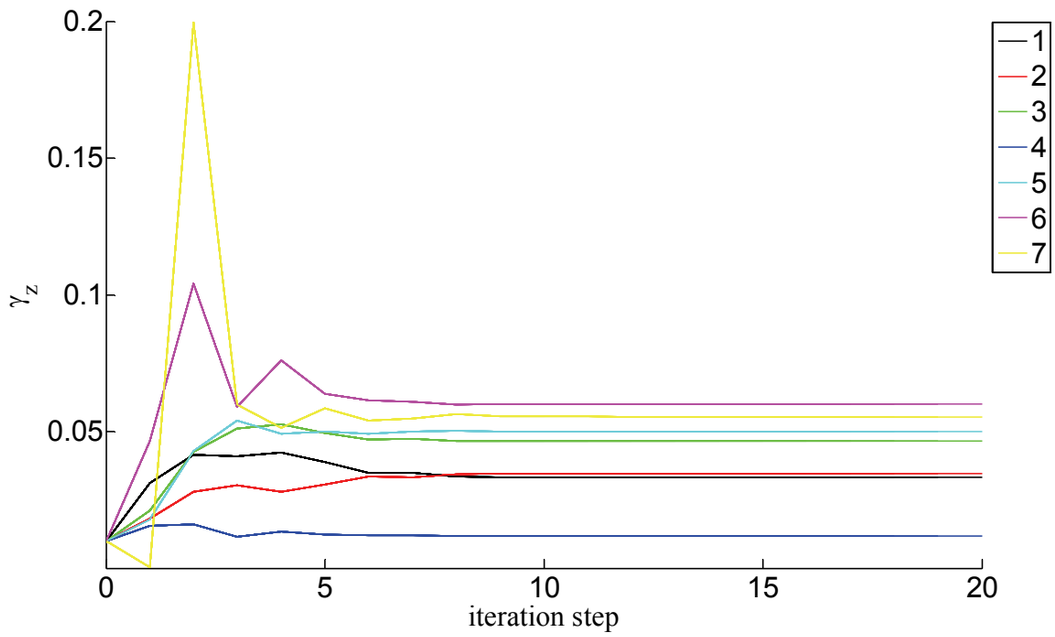

Fig. 7. Evolution of the damping parameters γ_z (z=1,...,7 in the legend) during iterations by adopting the proposed updating procedure. Example with 12 measurement response dofs and without noise.

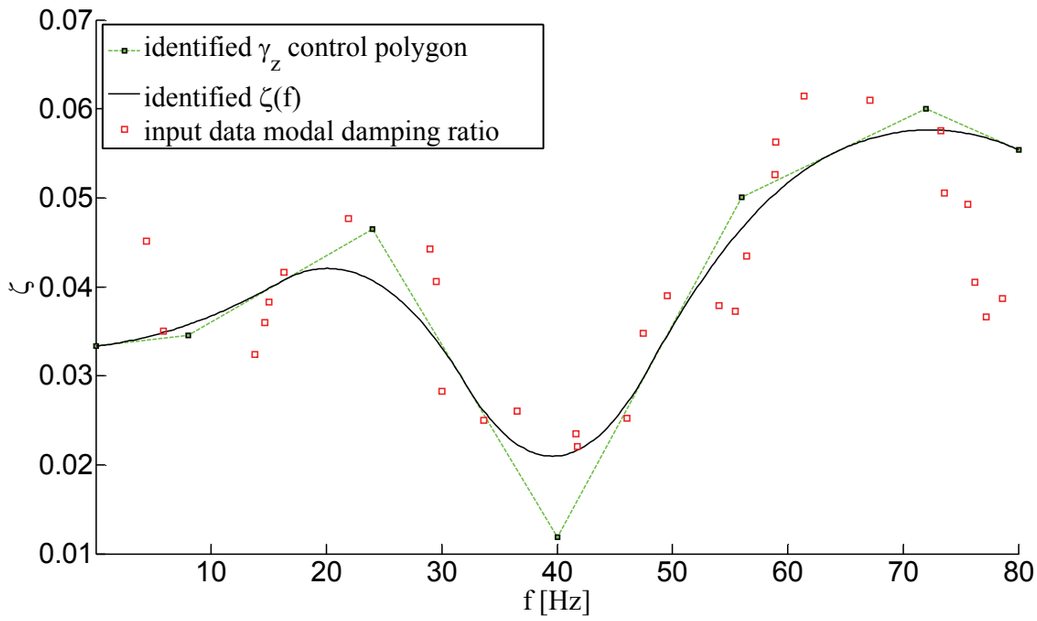

Fig. 8. Comparison of the modal damping ratio used to simulate the measurements (red squares) and the identified $\zeta(f)$ (black line; green filled squares refer to B-spline curve control coefficients). Example with 12 measurement response dofs and without noise.

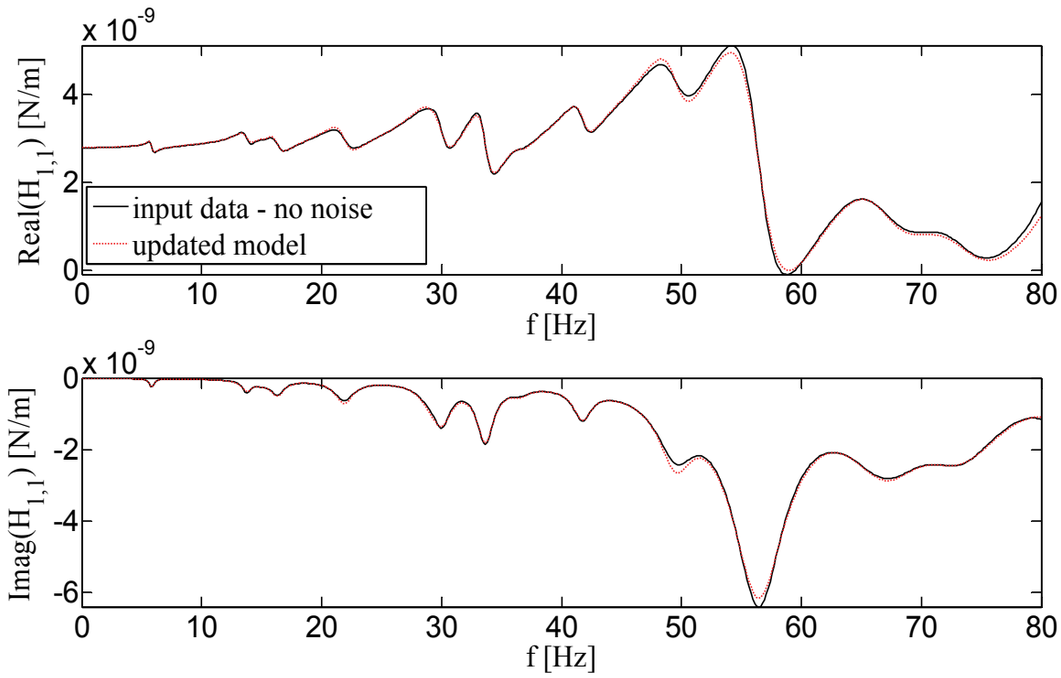

Fig. 9. Comparison of (input in point 1; output in point 1) FRF after updating (example with 12 measurement response dofs without noise): the input data (black continuous line) and the updated model (red dotted line).

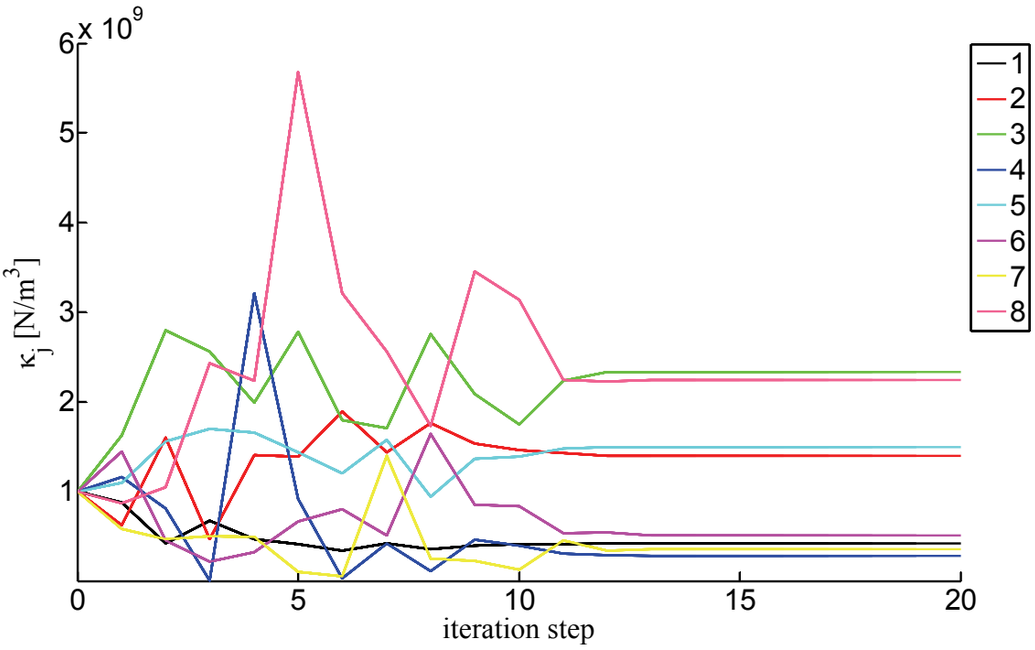

Fig. 10. Evolution of stiffness parameters κ_j (j=1,...,8 in the legend) during iterations by adopting the proposed updating procedure. Example with 4 measurement response dofs and without noise.

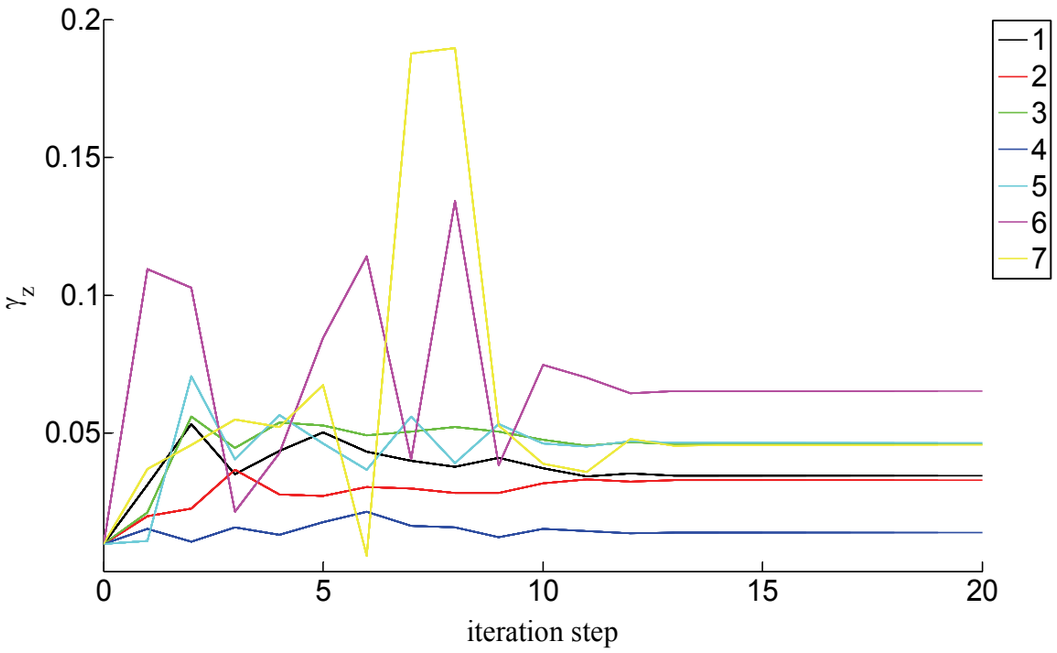

Fig. 11. Evolution of the damping parameters γ_z (z=1,...,7 in the legend) during iterations by adopting the proposed updating procedure. Example with 4 measurement response dofs and without noise.

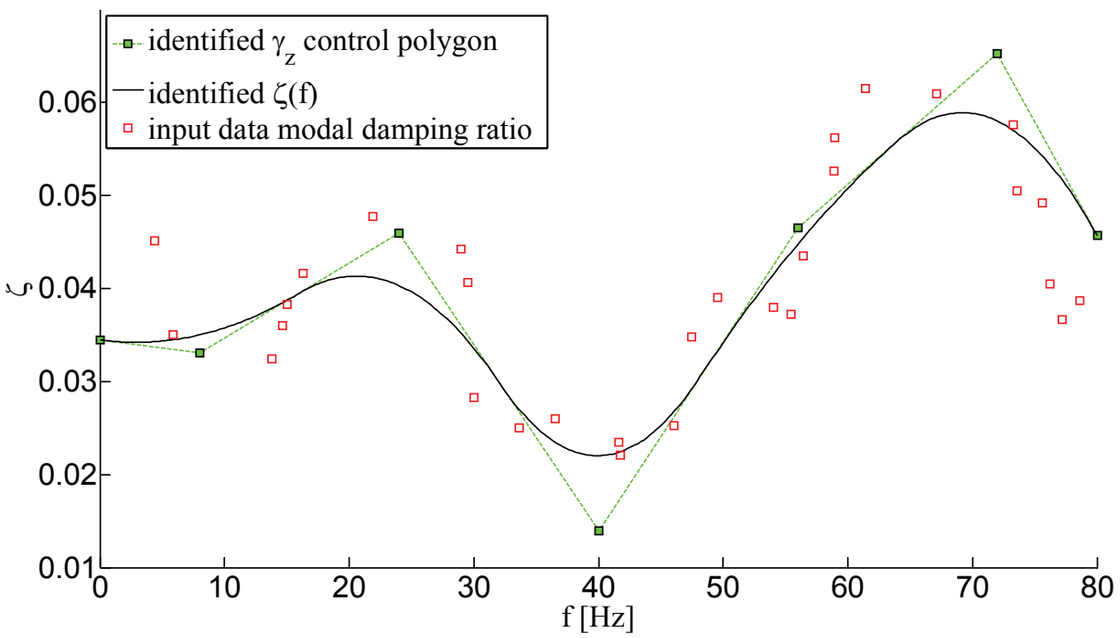

Fig. 12. Comparison of the modal damping ratio used to simulate the measurements (red squares) and the identified $\zeta(f)$ (black line; green filled squares refer to B-spline curve control coefficients). Example with 4 measurement response dofs and without noise.

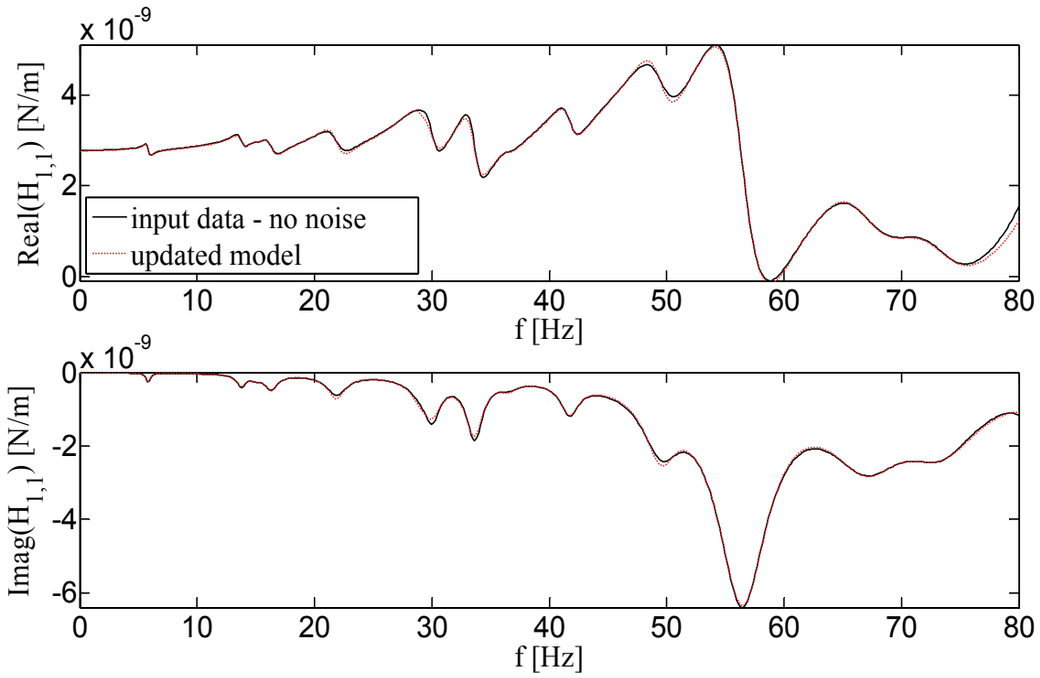

Fig. 13. Comparison of (input in point 1; output in point 1) FRF after updating (example with 4 measurement response dofs, without noise): the input data (black continuous line) and the updated model (red dotted line).

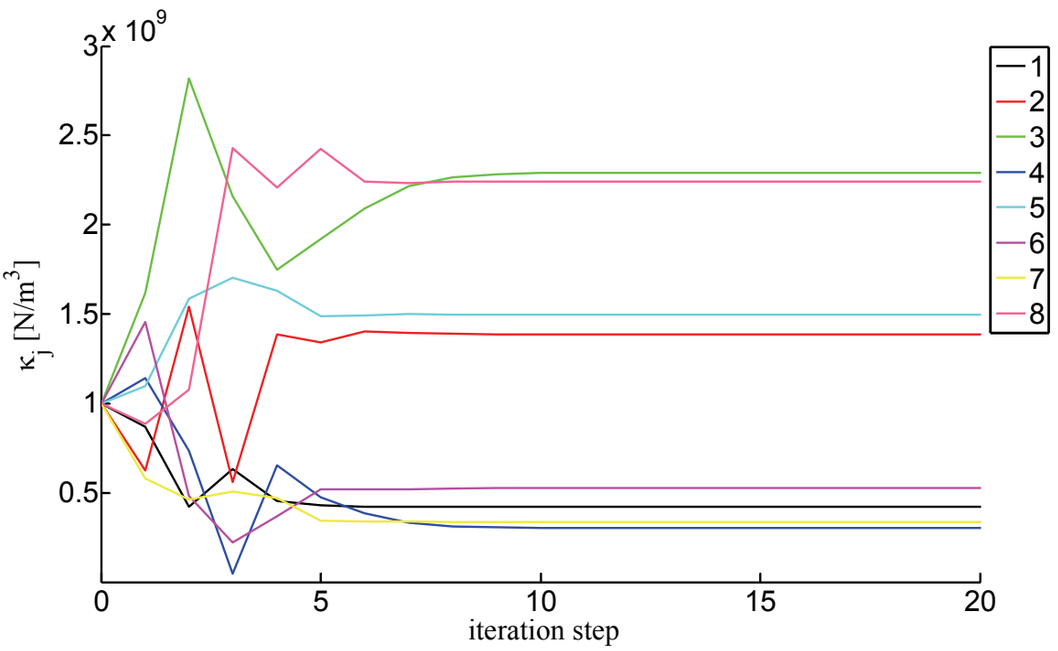

Fig. 14. Evolution of stiffness parameters κ_j (j=1,...,8 in the legend) during iterations by adopting the proposed updating procedure. Example with 4 measurement response dofs and with 3% noise.

4.3 Numerical simulations with noise

In these two simulations, the same updating parameters of the previous examples are considered with the same starting values. A random noise is added in FRFs, by considering a normal distribution with a standard deviation set to 3% and 10% of the signal RMS value. Four FRFs data (dofs from 1 to 4, Fig.2) are employed in the updating process.

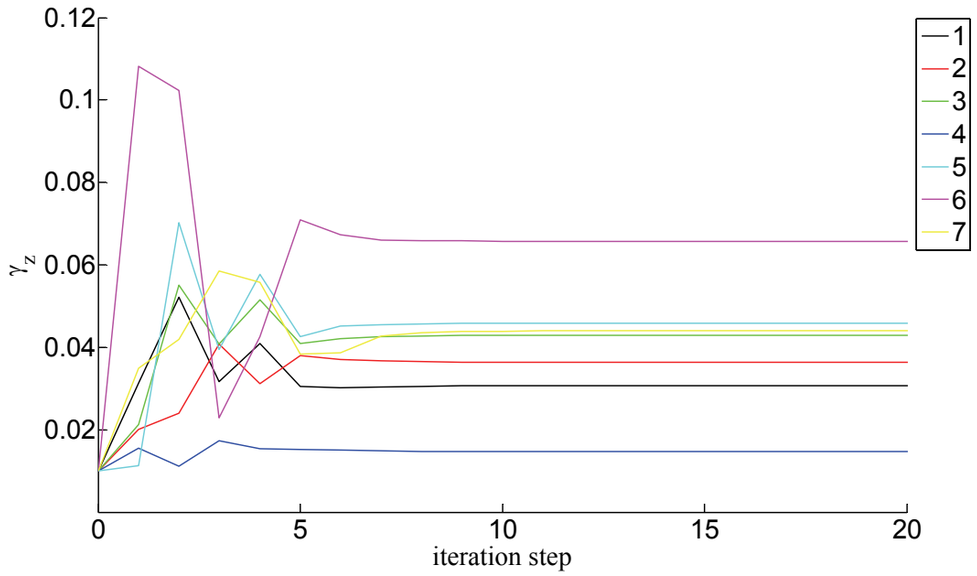

Fig. 15. Evolution of the damping parameters γ_z(z=1,...,7 in the legend) during iterations by adopting the proposed updating procedure. Example with 4 measurement response dofs and with 3% noise.

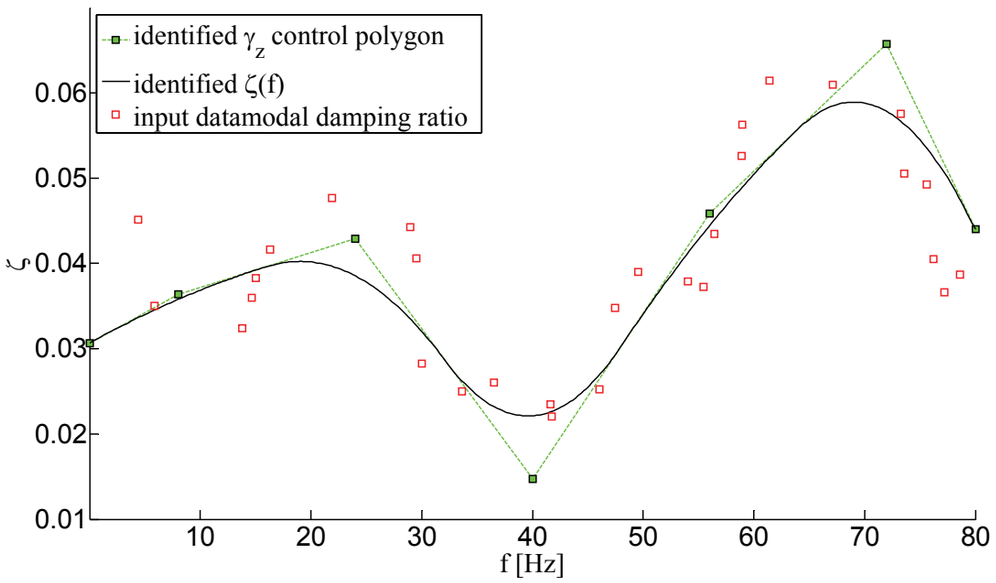

Fig. 16. Comparison of the modal damping ratio used to simulate the measurements (red squares) and the identified $\zeta(f)$ (black line; green filled squares refer to B-spline curve control coefficients). Example with 4 measurement response dofs and with 3% noise.

When 3% noise is added, the value of the identification parameters at each step, adopting the proposed procedure, is reported in Fig.14 for the stiffness coefficients, and in Fig.15 for the γ_z damping coefficients; Fig.16 refers to the comparison of the modal damping ratio used to simulate the measurements (red squares) and the identified curve (black line) where the green filled squares are the B-spline control coefficient γ_z. Fig.17 refers to the comparison of the input and updated FRFs.

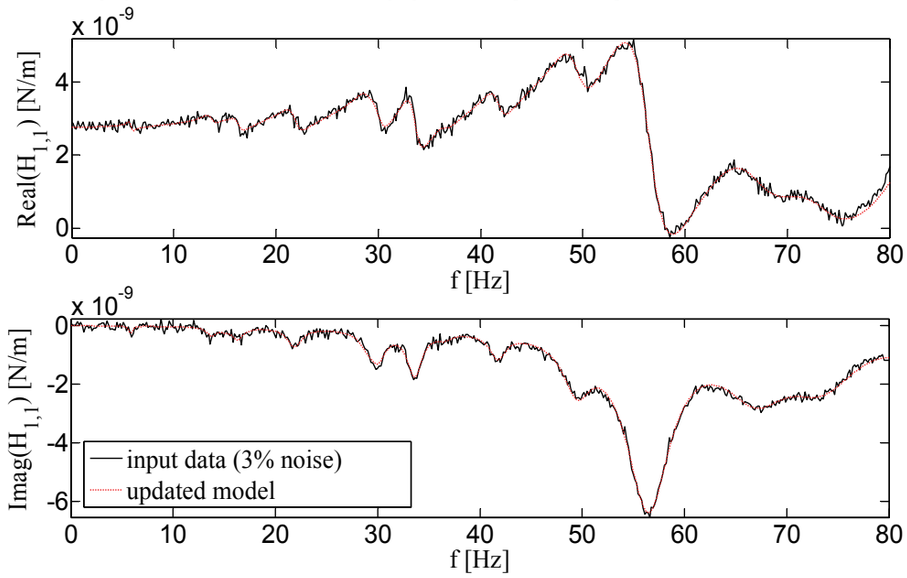

Fig. 17. Comparison of (input point 1; output point 1) FRF considering noise (3% case) after updating (4 measurement response dofs): the input data (black line) and the updated model (red line).

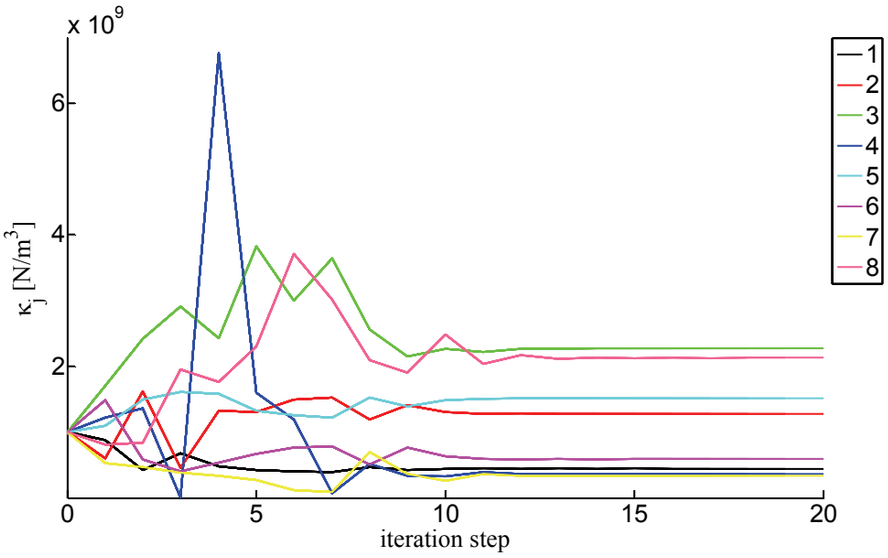

Fig. 18. Evolution of stiffness parameters κ_j (j=1,...,8 in the legend) during iterations by adopting the proposed updating procedure. Example with 4 measurement response dofs and with 10% noise.

For the simulation considering the 10% noise case, Fig.18 and Fig.19 show the evolution during iteration for, respectively, the stiffness coefficients and the γ_z damping coefficients; Fig.20 refers to the comparison of the modal damping ratio values used to simulate the measurements and the identified function. Fig.21 and Fig.22 refer to the comparison of the input and updated FRFs.

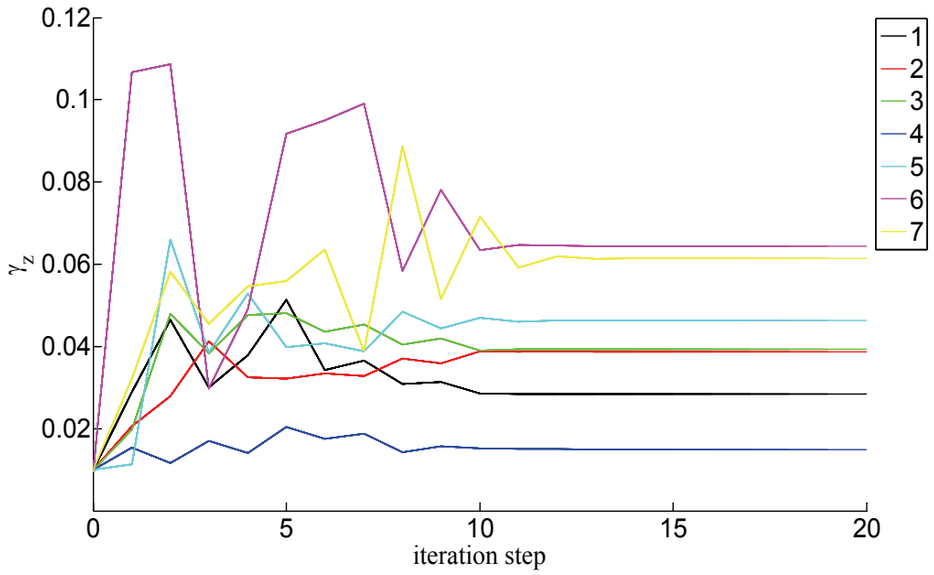

Fig. 19. Evolution of the damping parameters γ_z (z=1,...,7 in the legend) during iterations by adopting the proposed updating procedure. Example with 4 measurement response dofs and with 10% noise.

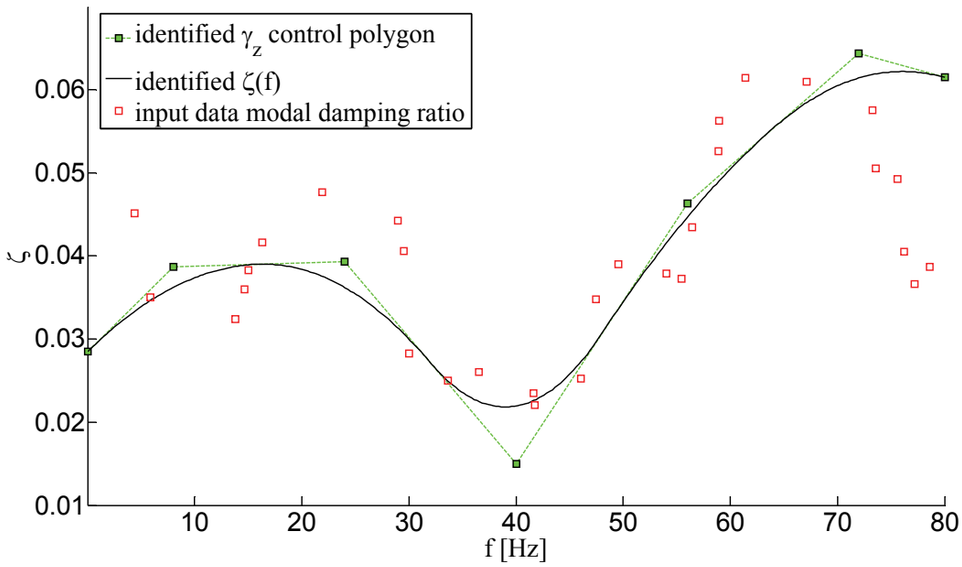

Fig. 20. Comparison of the modal damping ratio ζ used to simulate the measurements (red squares) with the identified $\zeta(f)$ (black line; green filled squares refer to B-spline curve control coefficients). Example with 4 measurement response dofs and with 10% noise.

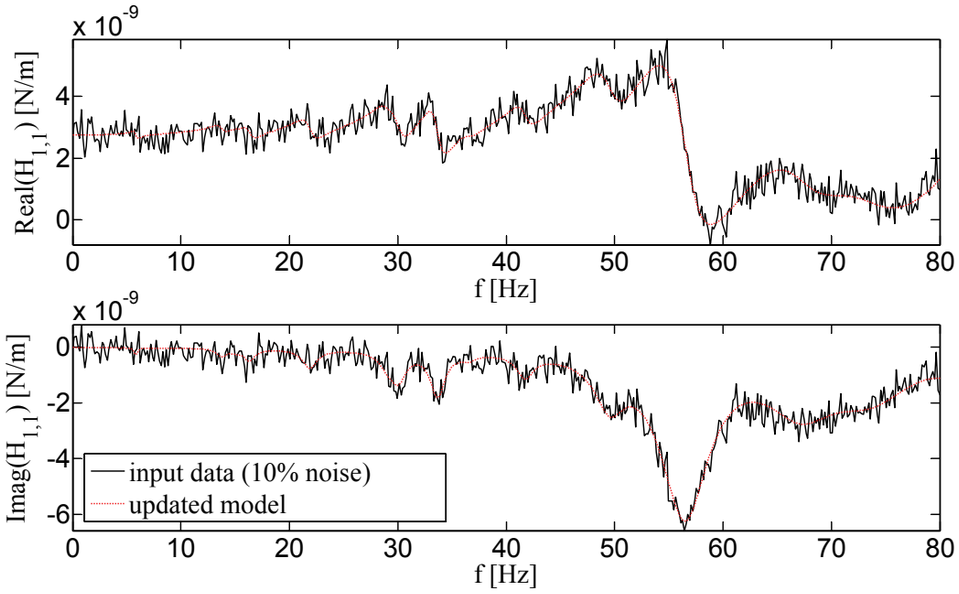

Fig. 21. Comparison of (input point 1; output point 1) FRF considering noise (10% case) after updating (4 measurement response dofs): the input data (black line) and the updated model (red line).

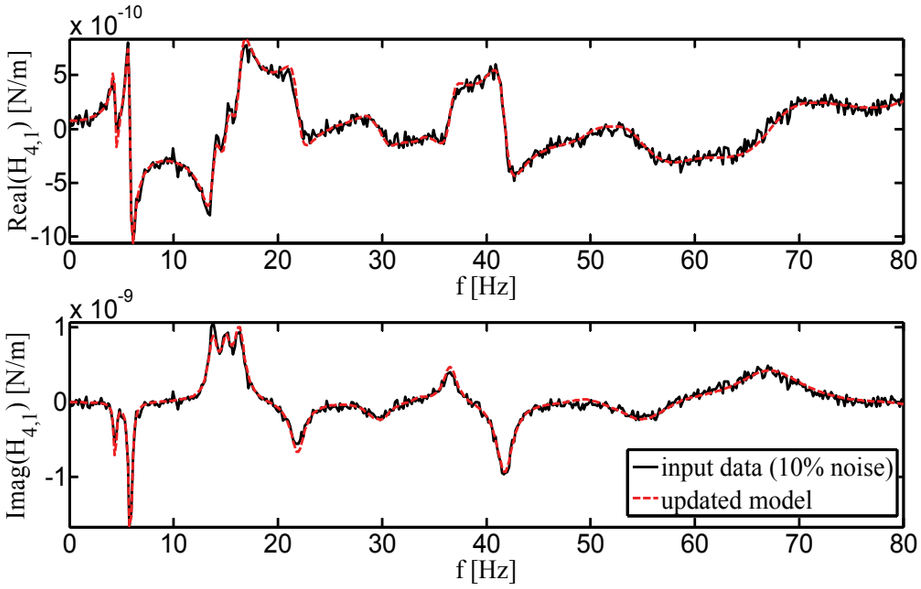

Fig. 22. Comparison of (input point 1; output point 4) FRF considering noise (10% case) after updating (4 measurement response dofs): the input data (black line) and the updated model (red line).

5. Discussion

Experimental measurement data were simulated by adopting the same B-spline analytical model used as the updating model. Numerical results showed good matching of the FRFs

after the updating process with both twelve and four measurement dofs, when noise is not considered. However, when only four measurement dofs are employed, more iterations were necessary to make updating parameter values become stable, with respect to the case in which twelve measurement dofs were adopted. The updated FRFs showed a good matching with the input FRFs even with the adoption of four measurement dofs and noisy data as input in the updating procedure: in the 10% noise case, the procedure required more iterations than in the 3% noise case example, but a moderately fast convergence was obtained anyway. A transformation of the updating variables was proposed to constrain the updated parameters to lie in a compact domain without using additional variables. This transformation ensured physical values to be assumed for all of the parameters during the iteration steps, and convergence was effectively and efficiently obtained in all of the cases under study.
The approach needs to be tested by adopting true measurement data as input. However, the experimental estimate of input-output FRFs for big structures like bridges can be difficult and can also be affected by experimental model errors, mainly due to input force placement, spatial distribution and measurement estimate. A technique employing output-only measured data need to be considered in future studies.

6. Conclusions

An updating procedure of a B-spline FE model of a railway bridge deck was proposed, the updating parameters being the coefficients of a distributed constraint stiffness model and the damping ratios, both modeled by means of B-spline functions. The optimization objective function was defined by considering the difference between the measured (numerically synthesised) FRFs and the linearized analytical FRFs. The incompatibility between the measured dofs and the non-physical B-spline FE model dofs was overcome by employing the same B-spline shape functions, thus adding a small computational cost.
A transformation of the updating variables was proposed to constrain the updated parameters to lie in a compact domain without using additional variables. Some test cases were investigated by simulating the experimental measurements by model based numerical simulations. Results are shown and critically discussed. Future applications will be addressed towards the development of a model updating technique employing output-only vibrational measured data.

7. Acknowledgments

The present study was developed within the MAM-CIRI, with the contribution of the Regione Emilia-Romagna, Progetto Tecnopoli. Support from the Italian Ministero dell'Università e della Ricerca (MIUR), under the "Progetti di Interesse Nazionale" (PRIN07) framework is also kindly acknowledged.

8. References

Carminelli, A. & Catania, G. (2007). Free vibration analysis of double curvature thin walled structures by a B-spline finite element approach. *Proceedings of ASME IMECE 2007*, pp. 1-7, Seattle (Washington), USA, 11-15 November 2007.

Carminelli, A. & Catania, G. (2009). PB-spline hybrid surface fitting technique. *Proceedings of ASME IDETC/CIE 2009*, pp.1-7, San Diego, California, USA, August 30-September 2, 2009.

Cook, R.D.; Malkus, D.S.; Plesha, M.E. & Witt, R.J. (1989). Concepts and applications of finite element analysis, J. Wiley & Sons, ISBN 0-471-35605-0, New York, NY, USA.

D'ambrogio W. & Fregolent A. (2000). Robust dynamic model updating using point antiresonances. *Proceedings of the 18th International Modal Analysis Conference*, pp. 1503-1512, San Antonio, Texas.

Esfandiari, A.; Bakhtiari-Nejad, F.; Rahai, A. & Sanayei, M. (2009). Structural model updating using frequency response function and quasi-linear sensitivity equation. *Journal of Sound and Vibration*, Vol. 326, 3-5, pp. 557-573, ISSN 0022-460X.

Friswell, M. I. & Mottershead, J. E. (1995) *Finite element modal updating in structural dynamics*, Kluwer Academic Publisher, ISBN 0-7923-3431-0, Dordrecht, Netherlands.

Friswell, M.I.; Mottershead, J.E. & Ahmadian, H. (2001). Finite-Element Model Updating Using Experimental Test Data: Parametrization and Regularization. *Philosophical Transactions: Mathematical, Physical and Engineering Sciences*, 359, 1778, Experimental Modal Analysis (Jan. 2001), pp. 169-186.

Gabriele S.; Valente, C. & Brancaleoni, F. (2009). Model calibration by interval analysis. *Proceedings of XIX AIMETA CONFERENCE*, Ancona, Italy, September 14-17, 2009.

Garibaldi, L.; Catania, G.; Brancaleoni, F.; Valente, C. & Bregant, L. (2005). Railway Bridges Identification Techniques. *Proceedings of IDETC2005: The 20th ASME Biennial Conference on Mechanical Vibration and Noise*, Long Beach, CA, USA, September 24-28, 2005.

Hughes, T.J.R.; Cottrell, J.A. & Bazilevs, Y. (2005). Isogeometric analysis: CAD, finite elements, NURBS, exact geometry, and mesh refinement. *Computer Methods in Applied Mechanics and Engineering*, 194, pp. 4135–4195, 2005.

Hughes, T.J.R.; Reali, A. & Sangalli, G. (2009). Isogeometric methods in structural dynamics and wave propagation, *Proceedings of COMPDYN 2009 - Computational Methods in Structural Dynamics and Earthquake Engineering*, Rhodes, Greece, 22-24 June 2009.

Lin, R.M. & Zhu, J. (2006). Model updating of damped structures using FRF data. *Mechanical Systems andSignal Processing*, 20, pp. 2200-2218.

Kagan, P. & Fischer, A. (2000). Integrated mechanically based CAE system using B-spline finite elements. Computer Aided Design, 32, pp. 539-552.

Piegl L. & Tiller, W. (1997). *The NURBS Book, 2nd Edition*. Springer-Verlag, ISBN 3-540-61545-8, New York, NY, USA.

Zapico, J.L.; Gonzalez, M.P.; Friswell, M.I.; Taylor, C.A. & Crewe, A.J. (2003). Finite element model updating of a small scale bridge. *Journal of Sound and Vibrations*, 268, pp. 993-1012.

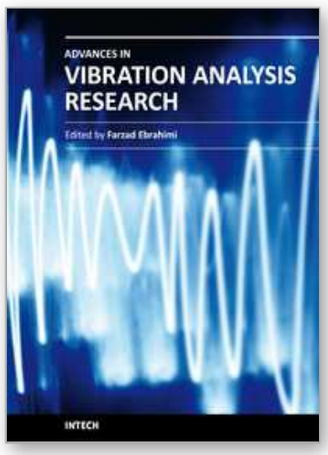

Advances in Vibration Analysis Research
Edited by Dr. Farzad Ebrahimi

ISBN 978-953-307-209-8
Hard cover, 456 pages
Publisher InTech
Published online 04, April, 2011
Published in print edition April, 2011

Vibrations are extremely important in all areas of human activities, for all sciences, technologies and industrial applications. Sometimes these Vibrations are useful but other times they are undesirable. In any case, understanding and analysis of vibrations are crucial. This book reports on the state of the art research and development findings on this very broad matter through 22 original and innovative research studies exhibiting various investigation directions. The present book is a result of contributions of experts from international scientific community working in different aspects of vibration analysis. The text is addressed not only to researchers, but also to professional engineers, students and other experts in a variety of disciplines, both academic and industrial seeking to gain a better understanding of what has been done in the field recently, and what kind of open problems are in this area.

How to reference
In order to correctly reference this scholarly work, feel free to copy and paste the following:

Antonio Carminelli and Giuseppe Catania (2011). B-spline Shell Finite Element Updating by Means of Vibration Measurements, Advances in Vibration Analysis Research, Dr. Farzad Ebrahimi (Ed.), ISBN: 978-953-307-209-8, InTech, Available from: http://www.intechopen.com/books/advances-in-vibration-analysis-research/b-spline-shell-finite-element-updating-by-means-of-vibration-measurements

INTECH
open science | open minds

InTech Europe
University Campus STeP Ri
Slavka Krautzeka 83/A
51000 Rijeka, Croatia
Phone: +385 (51) 770 447
Fax: +385 (51) 686 166
www.intechopen.com

InTech China
Unit 405, Office Block, Hotel Equatorial Shanghai
No.65, Yan An Road (West), Shanghai, 200040, China
中国上海市延安西路65号上海国际贵都大饭店办公楼405单元
Phone: +86-21-62489820
Fax: +86-21-62489821

IntechOpen